CFG-EC: ERROR CORRECTION CLASSIFIER FREE GUIDANCE

Nakkyu Yang Yechan Lee SooJean Han KAIST, Daejeon, Republic of Korea

{ynk6592, tuuktuc86, soojean}@kaist.ac.kr

November 19, 2025

Abstract

Classifier-Free Guidance (CFG) has become a mainstream approach for simultaneously improving prompt fidelity and generation quality in conditional generative models. During training, CFG stochastically alternates between conditional and null prompts to enable both conditional and unconditional generation. However, during sampling, CFG outputs both null and conditional prompts simultaneously, leading to inconsistent noise estimates between the training and sampling processes. To reduce this error, we propose CFG-EC, a versatile correction scheme augmentable to any CFG-based method by refining the unconditional noise predictions. CFG-EC actively realigns the unconditional noise error component to be orthogonal to the conditional error component. This corrective maneuver prevents interference between the two guidance components, thereby constraining the sampling error's upper bound and establishing more reliable guidance trajectories for high-fidelity image generation. Our numerical experiments show that CFG-EC handles the unconditional component more effectively than CFG and CFG++, delivering a marked performance increase in the low guidance sampling regime and consistently higher prompt alignment across the board.

1. Introduction

Diffusion models [6][21][23][24], which function by reversing a stochastic process that adds noise to data, represent a foundational class of modern generative models. Recent methods also focus on conditional generation, which integrates external conditions, such as class labels or text prompts, into the model to guide the output toward the desired attributes. In [2], a technique was used to guide the generation process by explicitly utilizing a pre-trained classifier, but this had the limitation that it required the additional training of a separate classifier model, which could also react unstably and unpredictably to the noisy input data in the diffusion process, thereby hindering the precision of the guidance.

A method is Classifier-Free Guidance (CFG) [5], a

technique that improves sample quality by interpolating between conditional and unconditional predictions without an additional classifier. This classifier-free approach is achieved by training the model to generate unconditional predictions, replacing text prompts in the training data with null tokens at a certain probability. However, this introduces a serious mismatch at sampling time. In contrast to the training phase, where conditional and unconditional noise predictions are learned separately, the CFG sampling process generates guidance by simultaneously producing and integrating these two distinct outputs. This fundamental difference causes the sampling process to deviate from the learned data distribution, forcing the model to operate in an out-of-distribution state not encountered during training. As a result, a discrepancy arises between the parameters optimized during training and those required for sampling. This problem cannot be solved by existing CFG correction methods [10][19][20].

In this work, we argue that a more robust solution requires moving beyond a reactive correction of errors toward a proactive correction. By correcting the model's unconditional prediction, our method resolves the instability at its source, guiding the generation process onto a more stable and higher fidelity, prompt aligned path. Our method reconceptualizes the guidance process by treating conditional and unconditional predictions as components within an error space. We actively reorient the unconditional prediction by nullifying its inherent errors. This technique provides a more stable unconditional signal that enhances the performance of guidance methods such as CFG [5] and CFG++ [1]. Theoretically, our approach reduces the upper bound on the sampling error, ensuring the model generation trajectory remains closer to the learned data manifold for more stable and reliable sampling. Empirically, our evaluation demonstrates that this active error correction guidance yields improvements in FID [4] and CLIP [17] scores. particularly in the low-guidance regime, while consistently increasing the CLIP score across all scales.

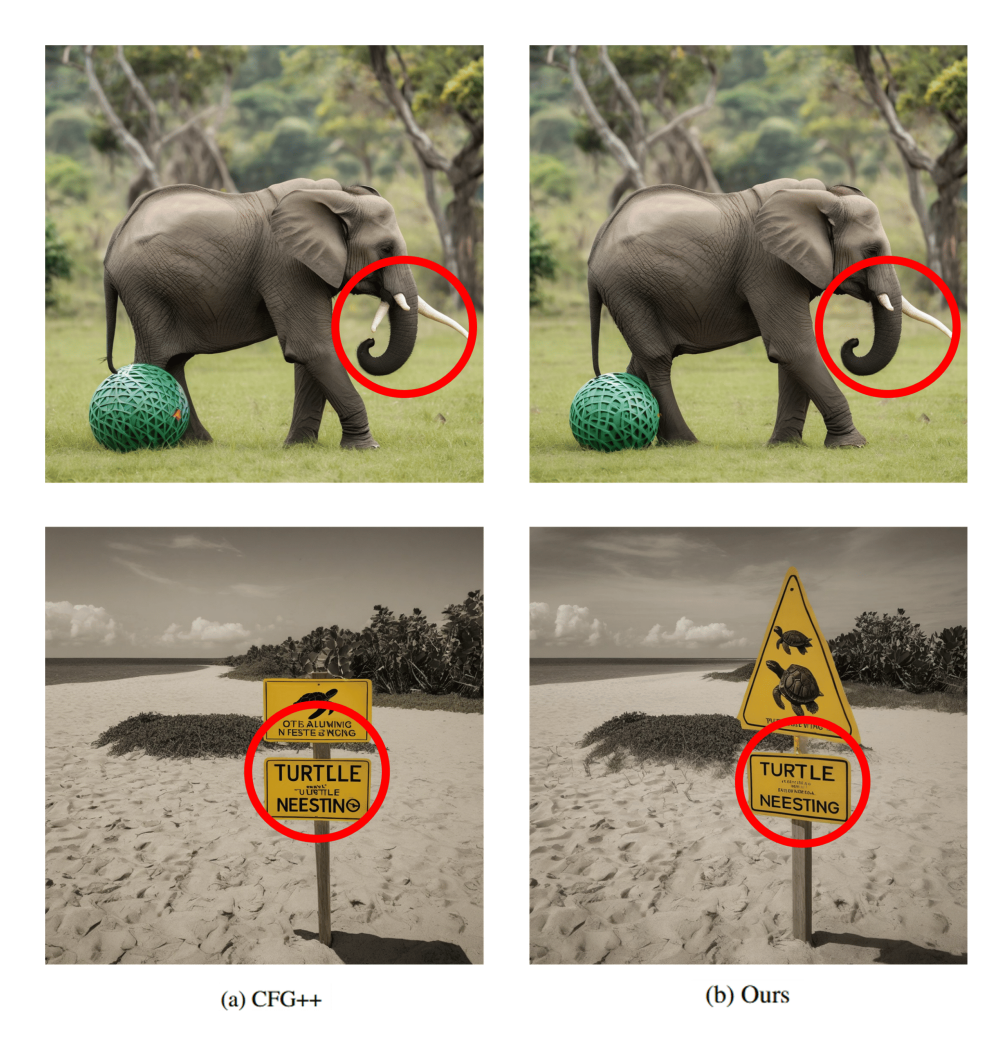


Figure 1. Comparison of Text-to-Image (T2I) generation results from Stable Diffusion XL [16] with DDIM [22] 50 NFEs, demonstrating our method's improved image fidelity. The CFG++ baseline (a) yields structural and textual artifacts (e.g., a third tusk, garbled text), our approach (b) achieves significantly higher visual fidelity and enhanced detail.

2. Related Work

2.1. Diffusion Model

Diffusion models [6][21][23][24] are a class of generative models that have demonstrated state-of-the-art performance in image generation and other domains. These models are characterized by two core processes: a forward process, which systematically corrupts data by adding Gaussian noise, and a reverse process, which learns to remove this noise to restore the original data from pure noise input. The forward process is defined as a Markov process that gradually adds noise to the initial data, x_0 , over a sequence of timesteps, t. This transition can be mathematically defined as follows.

$$x_t = \sqrt{\alpha_t} x_{t-1} + \sqrt{1 - \alpha_t} \epsilon$$
 where $\epsilon \sim \mathcal{N}(0, \mathbf{I})$

Expanding the recursive properties of the Markov chain extends the equation to the principle of additivity for Gaussian

distributions, which formalizes x_t as a linear combination of the initial data x_0 and a single equivalent Gaussian noise with accumulated variance. A key property of this process is that, starting from the initial data x_0 , it can be expressed in a closed form. This allows for direct sampling of the noisy state x_t at any arbitrary timestep, which can then be parameterized as follows.

$$q(x_t|x_0) = \mathcal{N}(x_t; \sqrt{\bar{\alpha}_t}x_0, (1-\bar{\alpha}_t)\mathbf{I})$$

Here, $\{\alpha_t\}_{t=1}^T$ is a predefined variance schedule such that $\alpha_t \in (0,1)$. This process is that we can sample x_t at any arbitrary timestep t directly from x_0 in a closed form. Letting $\bar{\alpha}_t = \prod_{s=1}^t \alpha_s$, this can also be parameterized by sampling a standard Gaussian noise vector $\epsilon \sim \mathcal{N}(0,\mathbf{I})$:

$$x_t = \sqrt{\bar{\alpha}_t} x_0 + \sqrt{1 - \bar{\alpha}_t} \epsilon$$

The training paradigm of denoising diffusion models is centered on predicting the noise that was added during a pre-

defined forward process. Specifically, a model $\epsilon_{\theta}(x_t,t)$ is optimized via a simple regression objective, mean squared error, to predict the true noise vector ϵ from a corrupted data sample x_t .

$$\mathcal{L}_{\text{simple}} = \mathbb{E}_{x_0, \epsilon, t} [\|\epsilon - \epsilon_{\theta}(x_t, t)\|^2]$$

Also the Gaussian noise's analytical tractability is crucial, as it enables a closed-form expression for the noisy sample distribution $q(x_t|x_0)$ and facilitates the reparameterization trick, both of which are essential for efficient training.

$$\nabla_{x_t} \log q(x_t|x_0) = -\frac{1}{1 - \bar{\alpha}_t} (x_t - \sqrt{\bar{\alpha}_t} x_0) = -\frac{1}{\sqrt{1 - \bar{\alpha}_t}} \epsilon$$

By substituting the parameterization $x_t = \sqrt{\bar{\alpha}_t} x_0 + \sqrt{1-\bar{\alpha}_t} \epsilon$, we find a direct relationship between the score function and the noise vector ϵ . Most critically, this Gaussian assumption provides a connection to score matching. The score function of the noised data distribution, $\nabla_{x_t} \log q(x_t|x_0)$, can be shown to be directly proportional to the negative of the added noise vector, i.e., $\nabla_{x_t} \log q(x_t|x_0) \propto -\epsilon$. Consequently, the simple task of predicting noise is equivalent to learning the score, which represents the underlying dynamics of the data distribution. This learned score function is then leveraged during the reverse process to guide a sample from a pure noise prior back to the data manifold, enabling high-fidelity generation.

2.2. Classifier-Free Guidance (CFG)

While unconditional models learn the overall data distribution p(x), many applications demand outputs conditioned on a specific prompt y (e.g., a class or text) [2]. To enable conditional generation in diffusion models, a technique known as classifier guidance is employed. This method leverages a score-based formulation of Bayes' theorem to steer the generation process. The core principle is that the score of the desired conditional distribution, $\nabla_x \log p(x|y)$, can be decomposed into two parts:

$$\underbrace{\nabla_x \log p(x|y)}_{\text{Conditional Score}} = \underbrace{\nabla_x \log p(x)}_{\text{Unconditional Score}} + \underbrace{\nabla_x \log p(y|x)}_{\text{Classifier Gradient}}$$

the score of the unconditional distribution, $\nabla_x \log p(x)$, and a guiding term derived from a classifier, $\nabla_x \log p(y|x)$. In practice, the pre-trained diffusion model provides an estimate for the unconditional score (related to its noise prediction) $\epsilon_\theta(x_t,t)$ [24], and this is combined with the gradient of the log-likelihood from an external, separately trained classifier that predicts the class y given a noisy input x. However, this approach introduces significant practical drawbacks. The most prominent disadvantage is that it necessitates training and maintaining two separate and distinct neural networks, such as the primary diffusion

model and an auxiliary classifier. The classifier must be specifically trained to be robust to the varying levels of noise present in the intermediate samples x, meaning a standard, pre-trained classifier cannot typically be used off-the-shelf. This requirement for two models, and the potential for misalignment between them, motivated the development of more computationally efficient approaches like Classifier-Free Guidance.

CFG was developed to simply estimate $\nabla_x \log p(y|x)$ without an external classifier. The training process incorporates a conditioning dropout scheme, where the provided condition y is randomly substituted with a null token (\varnothing) . This training method compels the network $\epsilon_{\theta}(x_t,t,y)$ to learn the conditional score $\nabla_x \log p(x|y)$ by constraining its optimization objective to the manifold of data corresponding to y. Also the network learns the unconditional score $\nabla_x \log p(x)$ when the condition alternates the null token (\varnothing) , enabling a single model to approximate both the conditional and unconditional score functions. From the score-based Bayes' rule, $\nabla_x \log p(x|y) - \nabla_x \log p(x) = \nabla_x \log p(y|x)$, the difference between the conditional and unconditional noise predictions implicitly provides the correction signal as an external classifier.

$$\epsilon_{\text{pred}} = \epsilon_{\text{uncond}} + w \cdot (\epsilon_{\text{cond}} - \epsilon_{\text{uncond}})$$

This formulation reinterprets the principles of classifier guidance. The term ϵ_{uncond} serves as an estimate of the unconditional score $\nabla_x \log p(x)$, establishing a baseline prediction, while ϵ_{cond} serves as an estimate of the conditional score $\nabla_x \log p(x|y)$. The scaled difference, $w \cdot (\epsilon_{\text{cond}} - \epsilon_{\text{uncond}})$, functions as the guidance vector. This vector is a classifier-free approximation of the conditional gradient $\nabla_x \log p(y|x)$, and the guidance scale w controls the strength of this conditioning, adjusting how strongly the output adheres to the condition y.

Subsequent research on CFG has focused on overcoming the limitations of the original method, specifically the trade-off between prompt alignment and image fidelity. A primary research direction addresses the "off-manifold" problem, where strong guidance scale pushes the generation process away from the data distribution, causing artifacts. CFG++ [1] resolves this issue by reformulating the guidance, which ensures the sampling trajectory remains on the learned data manifold. This results in improved sample quality, enables the use of lower guidance scales between 0 to 1, and enhances invertibility for image-editing tasks. Moreover, since a fixed guidance scale creates a suboptimal trade-off between fidelity and sample quality, another line of research involves making the guidance scale dynamic [8][9]. For instance, β -CFG [15] utilizes a time-dependent curve modeled by the Beta distribution to adaptively adjust guidance strength. This method stabilizes the guidance effect and optimizes the balance between text-image alignment and image fidelity. CFG-Zero* [3], designed for flow-matching models [12][13], observed that standard CFG can negatively impact performance in the early stages of generation when the model's velocity estimate is inaccurate. It introduces an optimized scaling factor and a "zero-init" scheme to deactivate guidance during the initial, most error-prone steps. On the other hand, Adaptive Projected Guidance (APG) [19], addresses the oversaturation and artifacts caused by high guidance scales. It achieves this by geometrically decomposing the guidance vector into components parallel and orthogonal to the conditional prediction. Based on the observation that the parallel component is the primary source of quality degradation, APG selectively downweights this component. This method reduces artifacts and generates more realistic images at high guidance scales.

3. Method

3.1. Understanding CFG Discrepancies: A Theoretical Analysis

CFG aims to ensure that the guided noise prediction, $\tilde{\epsilon}_{\theta_t}$, closely approximates the ground-truth noise ϵ_t^* conditioned on y,

$$\tilde{\epsilon}_{\theta}(x_t|y) \approx \epsilon^*(x_t|y)$$
 (1)

During training, the model minimizes the expected weighted sum of squared errors between unconditional and conditional predictions. The weighting parameter $p \in (0,1)$ denotes the probability of dropping the conditioning.

$$e_t^{\text{train}} = p \|\epsilon_{\theta}(x_t) - \epsilon^*(x_t)\|^2 + (1 - p) \|\epsilon_{\theta}(x_t|y) - \epsilon^*(x_t|y)\|^2$$

In contrast, during the sampling stage, both conditional and unconditional noise are drawn. Thus, sampling phase error is expressed as the norm of the combined error.

$$e_t^{\text{sample}}$$

$$= \|(1 - \omega)(\epsilon_{\theta}(x_t) - \epsilon^*(x_t)) + \omega(\epsilon_{\theta}(x_t|y) - \epsilon^*(x_t|y))\|^2$$

$$= (1 - \omega)^2 \|\epsilon_{\theta}(x_t) - \epsilon^*(x_t)\|^2 + \omega^2 \|\epsilon_{\theta}(x_t|y) - \epsilon^*(x_t|y)\|^2$$

$$+ 2\omega(1 - \omega)\langle\epsilon_{\theta}(x_t) - \epsilon^*(x_t), \epsilon_{\theta}(x_t|y) - \epsilon^*(x_t|y)\rangle$$
(3)

where ω is the guidance scale during sampling. The key discrepancy arises from the inner product term, which is present during the sampling but absent from the training.

To formally analyze the impact of this term, we adopt the standard assumption of the i.i.d. data distribution, where samples from the sampling process (x, y) are drawn from the same independent data distribution used during training. Under this assumption, we derive an upper bound for the sampling error $e_t^{\rm sample}$, which provides a theoretical foundation for designing sampling strategies that align with the model's learned behavior. To facilitate this analysis, we first re-express $e_t^{\rm sample}$ using a more general notation.

- Unconditional error vector: $\epsilon_{uc}^p = \epsilon_{\theta}(x_t) \epsilon^*(x_t)$
- Conditional error vector: $\epsilon_c^p = \epsilon_\theta(x_t|y) \epsilon^*(x_t|y)$
- Coefficients: $c=1-\omega, d=\omega$

Thus, the sampling error in Eq. (3) is $e_t = ||c\epsilon_{uc}^p + d\epsilon_c^p||^2$. By the Cauchy–Schwarz inequality,

$$\|c\epsilon_{uc}^p + d\epsilon_c^p\|^2 \le (c^2 + d^2)(\|\epsilon_{uc}^p\|^2 + \|\epsilon_c^p\|^2) \tag{4}$$

If positive scalars a, b satisfy

$$\|\epsilon_{uc}^p\|^2 + \|\epsilon_c^p\|^2 \le \frac{1}{\min(a^2, b^2)} (\|a\epsilon_{uc}^p\|^2 + \|b\epsilon_c^p\|^2),$$
 (5)

then

$$\|c\epsilon_{uc}^p + d\epsilon_c^p\|^2 \le \frac{c^2 + d^2}{\min(a^2, b^2)} (\|a\epsilon_{uc}^p\|^2 + \|b\epsilon_c^p\|^2)$$
 (6)

Setting $a = \sqrt{p}$ and $b = \sqrt{1-p}$ relates to the training error via Eq. (2), yielding the final sampling error bound:

$$e_t^{\text{sample}} \le \frac{(1-\omega)^2 + \omega^2}{\min(p, 1-p)} e_t^{\text{train}} \tag{7}$$

Alternatively, for orthogonal error vectors ($\langle \epsilon_{uc}^p, \epsilon_c^p \rangle = 0$), the sampling error bound becomes tighter

sample

$$= (1 - \omega)^2 \|\epsilon_{uc}^p\|^2 + \omega^2 \|\epsilon_c^p\|^2 \le \frac{\max((1 - \omega)^2, \ \omega^2)}{\min(p, 1 - p)} e_t^{\text{train}}$$
(8)

This analysis demonstrates that enforcing orthogonality between the unconditional and conditional error vectors eliminates the inner product term, resulting in a provably tighter upper bound on the sampling error. Unlike previous studies [1][3][5] that often implicitly assume that the training and sampling errors are identical, we explicitly characterize the discrepancy between them. Our analysis reveals that the sampling error can be bounded by the training error scaled by a factor. Furthermore, we demonstrate that this bound can be tightened by enforcing orthogonality between the error vectors.

Algorithm 1 Dynamic Error Correction Method

```
Input: Initial noise x_T, guidance scale w,
alignment threshold \tau, conditional noise at t\epsilon_t^{(c)},
unconditional noise at t\epsilon_t^{(uc)}
    1: for t = T to 1 by -1 do
                 if t < T then
                       // Extrapolate to define error vectors
   3:
                     .. Exampliate to define error vectors A \leftarrow \epsilon_t^{(c)} - (\tilde{\epsilon}_{t-1}^{(c)} \approx (2\epsilon_t^{(c)} - \epsilon_{t+1}^{(c)})) B \leftarrow \epsilon_t^{(uc)} - (\tilde{\epsilon}_{t-1}^{(uc)} \approx (2\epsilon_t^{(uc)} - \epsilon_{t+1}^{(uc)})) s = \frac{\langle A, B \rangle}{\|A\| \|B\|}
   5:
    6:
                       if s < \tau then
    7:
                            // Correct unconditional via Gram-Schmidt B_{\perp} \leftarrow B - \frac{\langle A,B \rangle}{\|A\|^2} A \epsilon_{uc, \text{modified}} \leftarrow (B_{\perp}) + (\tilde{\epsilon}_{t-1}^{(uc)} \approx (2\epsilon_t^{(uc)} - \epsilon_{t+1}^{(uc)}))
   8:
    9:
  10:
                            // Dynamic interpolation method \epsilon_t^{(uc)} \leftarrow (1-s) \cdot \epsilon_{uc, \text{modified}} + s \cdot \epsilon_t^{(uc)}
 11:
  12:
  13:
  14:
                 end if
                 // Standard CFG with corrected unconditional
  15:
                \begin{aligned} & \kappa_t^{(pred)} \leftarrow \epsilon_t^{(uc)} + w(\epsilon_t^{(c)} - \epsilon_t^{(uc)}) \\ & \text{// Update the state using a generic sampler step} \\ & x_{t-1} \leftarrow Solver(x_t, \epsilon_t^{(pred)}) \end{aligned}
  16:
  18:
  19: end for
 20: return Decoded image from x_0
```

3.2. Implementation of Error Correction Sampling

The ground-truth noise error is inaccessible during sampling. Therefore, we introduce an error proxy derived from the time-step difference of the model's predictions. For both the conditional and unconditional predictions, we define an "error vector" as the difference between the noise predicted at the current step and an extrapolated prediction for the subsequent step. The key intervention of our method is to then apply the Gram-Schmidt [25] process to these two error vectors. Because modifying the conditional noise prediction causes the generative process to deviate from the prompt condition and thus degrade fidelity, we instead adjust the unconditional noise to enhance generation quality. By applying this correction, the unconditional noise prediction is adjusted so that its corresponding unconditional error vector becomes orthogonal to the conditional error vector. This purposefully minimizes the inner product term, which constitutes an error source in CFG, we define the ensuing configuration as the "Full method", to reflect that it does not utilize the model's original unconditional noise output but instead integrates the entirely modified unconditional noise.

The original predictions of the model faithfully capture the intricate distribution of the training data, thereby con-

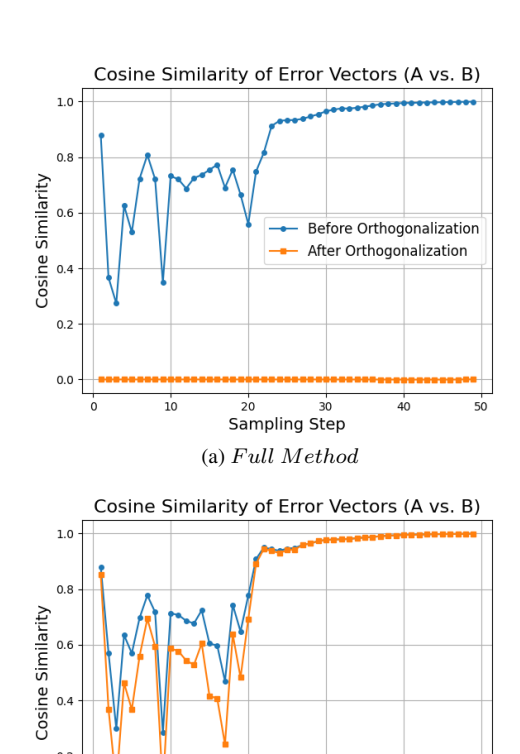


Figure 2. Cosine similarity of the error vectors before and after correction by each method. The Full Method (a) sets the cosine similarity to 0, whereas the Dynamic Method (b) adaptively adjusts it to dynamically control the strength of the correction.

(b) Dynamic Method

Before Orthogonalization After Orthogonalization

taining the most granular details, such as subtle textures, complex lighting, and fine-scale patterns. However, these fine-grained features are susceptible to degradation during post-processing for mismatch correction. To resolve the inherent trade-off between discrepancy correction and detail preservation, we introduce a dynamic interpolation algorithm. The mixing ratio is directly governed by the cosine similarity between the error vectors, which acts as an indicator of the utility of the Gram-Schmidt correction at each step. The algorithm assigns weights giving the original noise the cosine similarity value and the corrected noise its complement. As two error vectors are aligned and cosine similarity approaches 1, the Gram-Schmidt correction converges to 0, eliminating the directional correction's effectiveness. Furthermore, shifting the predicted value to the extrapolated target point without any directional correction can lead to unnecessary deviations from the model's original predictions, leading to instability and potentially damaging the original's intrinsic information.

tively regulates the aggressive shift towards the unstable, extrapolated target, thereby ensuring overall stability. This method is also controlled by a deactivation threshold, which bypasses the corrective process for a step if the cosine similarity exceeds a preset limit (e.g., 0.8 or 0.9). This threshold ensures that the algorithm not only dynamically balances correction and preservation through proportional blending but also ceases intervention entirely when it becomes unnecessary, thus preventing over-correction and preserving essential detail.

The Fig. 2 illustrates the cosine similarity trajectory of the error vectors for the same caption, "A small cactus with a happy face in the Sahara desert", presenting a compelling comparison between a full method, mathematical orthogonalization method and a dynamic interpolation method. The graph on the top illustrates a strict orthogonalization, full method. The "After Orthogonalization" line in the cosine similarity plot remains perfectly zero throughout the sampling process. This demonstrates that the algorithm has completely removed the component of the unconditional error vector that is parallel to the conditional error vector. This method risks discarding subtle details that contribute to the final image's overall realism.

In contrast, as visualized in the graph at the bottom, the "After Orthogonalization" line in the cosine similarity plot does not drop to zero. It dynamically follows a path below the "Before" line, indicating that the interference between the error vectors is reduced but not entirely eliminated. This behavior suggests that the algorithm uses the cosine similarity as a signal to intelligently modulate the strength of the correction.

4. Experiment

4.1. Experimental Settings

In this section, we design an experiment to effectively demonstrate the performance improvement of our proposed method, CFG-EC, over the existing CFG and CFG++. The main experiment is conducted on Stable Diffusion XL [16] and Stable Diffusion v1.5 [18]. We use three samplers, where DDIM [22] is run with 50 NFEs and UniPC [26] and DPM-Solver++(2M) [14] are run with 20 NFEs. To evaluate the performance of our algorithm on the Text-to-Image (T2I) task, we generate images using the first prompt from the MSCOCO captions [11]. The performance is measured using FID [4] and CLIP [17] scores.

4.2. Results

To empirically validate the efficacy of our proposed method, we conduct a quantitative evaluation across different guidance scales against established baselines, CFG and CFG-EC. The experiments are performed on the MSCOCO 10k validation set. We employ the DPM-Solver++(2M)sampler with 20 NFEs with the Karras sigma schedule [7]. The results, presented in Tab. 1, demonstrate the compelling advantages of our proposed method, "Ours (Full)". The most striking outcome is observed in the low-guidance regime, specifically at $\omega = 0.5$, where our method achieves an FID score of 56.31, a dramatic improvement of over 8.4 points compared to the standard CFG baseline (64.74). The experimental results show that the "Full" method, which completely eliminates the inner product of the error vectors, achieves higher CLIP scores than the CFG, indicating better prompt alignment. At higher guidance scales (e.g., $\omega = 2.5$), however, the improvement in CLIP comes at the expense of the FID score, reflecting a trade-off between prompt alignment and the presence of artifacts. In contrast, our proposed "Dynamic" algorithm presents a calibrated compromise. With the exception of the 2.5 guidance scale, this method simultaneously improves both the FID and CLIP on other tested scales. This demonstrates its efficacy as a balanced approach that enhances both generation reality and prompt adherence without the sacrifices inherent in the "Full" method.

The superior performance of our method, particularly at low guidance scales, can be attributed to its core mechanism. This mechanism directly refines the unconditional noise prediction. In settings where the guidance scale ω is small (e.g., $\omega=0.5$), the overall magnitude of the guidance vector term is inherently limited, making the quality of the final output highly dependent on the accuracy of the unconditional prediction. Our approach modifies this unconditional component to produce a more stable and coherent noise estimate. Also the modified guidance vector, derived from the adjusted unconditional prediction, successfully improves prompt adherence, as evidenced by higher CLIP scores across the board.

Motivated by effectiveness at low guidance via improved unconditional noise prediction, we embed our "Dynamic" method into the CFG++ framework, which already leverages unconditional estimates at lower scales. We refer to this modified version as CFG-EC++, integrating our modified unconditional and conditional predictions, and empirically compare it against CFG++. A quantitative evaluation was conducted to the Stable Diffusion v1.5 model with a 50-step DDIM sampler to generate images from MSCOCO 10k validation set. As shown in Tab. 2, compared to the baseline CFG++ in three of the five tested configurations ($\omega = 0.2$, 0.4, 0.6), our method successfully overcomes the fidelity-

	$\omega = 0.5$		$\omega = 2.5$		$\omega = 5.0$		$\omega = 7.5$	
Method	FID ↓	CLIP ↑	FID ↓	CLIP ↑	FID ↓	CLIP ↑	FID↓	CLIP ↑
CFG [5]	64.74	21.23	13.18	31.05	15.81	31.75	18.62	31.87
CFG-EC (Dynamic)	62.52	21.50	13.23	31.09	15.77	31.86	18.59	31.96
CFG-EC (Full)	56.31	22.32	14.09	31.29	16.23	32.16	18.91	32.18

Table 1. Quantitative evaluation of the DPM-Solver++(2M) 20 NFEs on MSCOCO 10k dataset.

	ω =	= 0.2	ω =	= 0.4	ω =	= 0.6	ω =	= 0.8	ω =	= 1.0
Method	FID ↓	CLIP↑	FID ↓	CLIP↑	FID ↓	CLIP↑	FID ↓	CLIP↑	FID↓	CLIP↑
CFG++ [1] CFG-EC++ (Dynamic)				31.79 31.85						

Table 2. Quantitative evaluation of 50 NFEs DDIM T2I with SD v1.5 on MSCOCO 10k dataset.

alignment trade-off, simultaneously achieving a lower FID score and a higher CLIP score. The most significant performance gain is observed at $\omega=0.4$, where our method reduces FID by 0.12 while also improving the CLIP score. At the highest tested values $\omega=0.8$, 1.0, a slight trade-off emerges where fidelity is marginally compromised for a continued improvement in text alignment.

The performance difference is most pronounced near the $\omega=0.4,\,0.6$ mark, which corresponds to the region where our proposed guidance modification term, proportional to $2\omega(1-\omega)$ in the inner-product coefficient of Eq. (3), is maximized (peaking at $\omega=0.5$) between 0 and 1. Additionally, at guidance scales of 0.8 and 1.0, a CLIP score improvement occurred at the cost of a marginal FID degradation, consistent with the minimal adjustment specified in Eq. (7) and Eq. (8). The empirical results, which align with our theoretical predictions, validate the efficacy of the proposed mechanism and rule out coincidental factors.

Model	Method (Guidance Scale)	$FID(\downarrow)$	$CLIP(\uparrow)$
SD v1.5 (UniPC)	CFG (0.6)	75.15	22.84
SD v1.5 (UniPC)	CFG-EC (Full) (0.6)	71.14	23.32
SD v1.5 (UniPC)	CFG (0.8)	50.06	26.35
SD v1.5 (UniPC)	CFG-EC (Full) (0.8)	48.99	26.44
SD v1.5 (DPM++ 2M)	CFG++ (0.5)	13.15	30.85
SD v1.5 (DPM++ 2M)	CFG-EC++ (Dynamic) (0.5)	13.14	30.91
SDXL (DDIM)	CFG++ (0.5)	23.17	31.87
SDXL (DDIM)	CFG-EC++ (Dynamic) (0.5)	23.11	31.95

Table 3. Quantitative comparison on the MSCOCO dataset on T2I sampling

As presented in Tab. 3, our proposed method demonstrates consistent improvements when applied to both the standard CFG and the enhanced CFG++ baselines across diverse experimental settings. On the MSCOCO 10k dataset with the SD v1.5 model and UniPC solver, our

approach was first evaluated against the standard CFG. At a 0.6 guide scale, it reduced the FID score from 75.15 to 71.14 and increased the CLIP score from 22.84 to 23.32. A similar advantage was observed on a higher guidance scale of 0.8. To demonstrate broader compatibility, we extended the various evaluations to the CFG++ baseline. Using the DPM++ 2M solver with SD v1.5 on the same dataset, our method improved the CLIP score from 30.85 to 30.91 while maintaining a nearly identical FID score. Furthermore, on the MSCOCO 5K dataset with the SDXL model and DDIM solver, our method again enhanced the CFG++ baseline, decreasing the FID score from 23.17 to 23.11 and increasing the CLIP score from 31.87 to 31.95.

4.3. Ablation Study

To validate the efficacy and necessity of the dynamic mixing strategy, we conducted an ablation study across three distinct variants of our method. Each variant is defined by how it constructs the unconditional prediction from the original and orthogonalized to the conditional error vector.

The experimental settings are as follows.

CFG-EC++ (**Full**): A strategy that uses only the fully modified unconditional prediction by ensuring that the unconditional error vector is orthogonal to the conditional error vector.

CFG-EC++ (0.7): Fixed-Ratio Mixing: A static strategy that blends the modified and original predictions using a fixed ratio (30% and 70% respectively), which was found to be empirically effective.

CFG-EC++ (**Dynamic**): Our proposed method adaptively adjusts the mixing ratio based on the cosine similarity between the conditional and unconditional error vectors.

Method	FID Score (\(\psi \)	CLIP Score (†)
CFG-EC++ (Full)	19.04	32.25
CFG-EC++ (0.7)	18.78	32.04
CFG-EC++ (Dynamic)	18.73	32.01

Table 4. Quantitative comparison on the MSCOCO 10k on SD v1.5 in 0.6 guidance scale with the DDIM 50 NFEs



(a) CFG++



(b) Ours

Figure 3. Comparison of SDXL T2I generation with the DDIM 50 NFEs. The baseline (a) exhibits a significant structural artifact, featuring a physically incorrect railway track. In contrast, the result in (b) presents a coherent structure.

The results in Tab. 4. reveal a trade-off between prompt alignment and image fidelity. The Full orthogonalization strategy attains the highest CLIP score (32.25), suggesting that eliminating directional interference maximizes adherence to the text prompt. However, this aggressive correction comes at the cost of image fidelity, yielding the lowest FID score (19.04). Conversely, the Fixed-Ratio Mixing strategy improves the FID score to 18.78, but this static compromise slightly dilutes the guidance signal,

resulting in a lower CLIP score. The proposed Dynamic method achieves the best FID score (18.73), indicating superior image quality and realism, while simultaneously maintaining a competitive CLIP score (32.01) that is nearly on par with the fixed-ratio approach.

These results empirically validate our core hypothesis. An adaptive mechanism that calibrates the corrective intervention based on the evolving state of error vectors is superior to static approaches. Our method attains a superior balance between visual fidelity, as measured by FID, and text-image alignment, indicated by CLIP scores. This result validates the role of our dynamic control strategy as a core and indispensable element of the algorithm.

5. Conclusion

This research addresses quality degradation in Classifier-Free Guidance (CFG) caused by an uncontrolled inner product term arising from discrepancies between the training and sampling processes. While existing methods mitigate symptoms by scaling guidance vectors, this study actively corrects the noise prediction to address the problem's root cause. We propose a novel sampling algorithm that approximates error vectors at each step and applies Gram-Schmidt orthogonalization to modify the unconditional noise prediction. This forces the error vectors toward an orthogonal relationship, neutralizing the inner product term responsible for error. Experimental results not only demonstrate performance improvements over conventional CFG, particularly in the low-guidance regime where unconditional prediction quality is critical, but also confirm a consistent enhancement in prompt alignment across all guidance scales, validating the method's ability to steer generation toward the intended output. We attribute this enhancement to the direct correction of systematic discrepancies introduced by the dropout mechanism, which identify a mismatch between training and sampling and have been overlooked in prior work. This approach directly addresses the instability that plagues existing methods, suggesting a direction for more robust diffusion models.

References

- [1] Hyungjin Chung, Jeongsol Kim, Geon Yeong Park, Hyelin Nam, and Jong Chul Ye. Cfg++: Manifold-constrained classifier free guidance for diffusion models. In *International Conference on Learning Representations*, 2025. 1, 3, 4, 7, 10
- [2] Prafulla Dhariwal and Alexander Nichol. Diffusion models beat gans on image synthesis. In *Advances in Neural Information Processing Systems*, pages 8780–8794, 2021. 1, 3
- [3] Weichen Fan, Amber Yijia Zheng, Raymond A Yeh, and Ziwei Liu. Cfg-zero*: Improved classifier-free guidance for flow matching models. 2025. 4
- [4] Martin Heusel, Hubert Ramsauer, Thomas Unterthiner, Bernhard Nessler, and Sepp Hochreiter. Gans trained by a two time-scale update rule converge to a local nash equilibrium. In Advances in Neural Information Processing Systems, 2017. 1, 6
- [5] Jonathan Ho and Tim Salimans. Classifier-free diffusion guidance. In Advances in Neural Information Processing Systems, 2021. 1, 4, 7, 10
- [6] Jonathan Ho, Ajay Jain, and Pieter Abbeel. Denoising diffusion probabilistic models. In *Advances in Neural Information Processing Systems*, pages 6840–6851, 2020. 1, 2
- [7] Tero Karras, Miika Aittala, Timo Aila, and Samuli Laine. Elucidating the design space of diffusion-based generative models. In Advances in Neural Information Processing Systems, pages 26565–26577, 2022. 6
- [8] Felix Koulischer, Johannes Deleu, Gabriel Raya, Thomas Demeester, and Luca Ambrogioni. Dynamic negative guidance of diffusion models. In *International Conference on Learning Representations*, 2025. 3
- [9] Tuomas Kynkäänniemi, Miika Aittala, Tero Karras, Samuli Laine, Timo Aila, and Jaakko Lehtinen. Applying guidance in a limited interval improves sample and distribution quality in diffusion models. In *Advances in Neural Information Processing Systems*, pages 122458–122483, 2024. 3
- [10] Shanchuan Lin, Bingchen Liu, Jiashi Li, and Xiao Yang. Common diffusion noise schedules and sample steps are flawed. In *Proceedings of the IEEE/CVF Winter Conference on Applications of Computer Vision*, pages 5404–5411, 2024. 1
- [11] Tsung-Yi Lin, Michael Maire, Serge Belongie, James Hays, Pietro Perona, Deva Ramanan, Piotr Dollár, and C Lawrence Zitnick. Microsoft coco: Common objects in context. In European Conference on Computer Vision, pages 740–755, 2014. 6
- [12] Yaron Lipman, Ricky TQ Chen, Heli Ben-Hamu, Maximilian Nickel, and Matt Le. Flow matching for generative modeling. In *International Conference on Learning Representations*, 2023. 4
- [13] Yaron Lipman, Marton Havasi, Peter Holderrieth, Neta Shaul, Matt Le, Brian Karrer, Ricky TQ Chen, David Lopez-Paz, Heli Ben-Hamu, and Itai Gat. Flow matching guide and code. arXiv preprint arXiv:2412.06264, 2024. 4
- [14] Cheng Lu, Yuhao Zhou, Fan Bao, Jianfei Chen, Chongxuan Li, and Jun Zhu. Dpm-solver++: Fast solver for guided sam-

- pling of diffusion probabilistic models. *Machine Intelligence Research*, pages 1–22, 2025. 6
- [15] Dawid Malarz, Artur Kasymov, Maciej Zięba, Jacek Tabor, and Przemysław Spurek. Classifier-free guidance with adaptive scaling. 2025. 3
- [16] Dustin Podell, Zion English, Kyle Lacey, Andreas Blattmann, Tim Dockhorn, Jonas Müller, Joe Penna, and Robin Rombach. Sdxl: Improving latent diffusion models for high-resolution image synthesis. In *International Con*ference on Learning Representations, 2024. 2, 6, 10
- [17] Alec Radford, Jong Wook Kim, Chris Hallacy, Aditya Ramesh, Gabriel Goh, Sandhini Agarwal, Girish Sastry, Amanda Askell, Pamela Mishkin, Jack Clark, et al. Learning transferable visual models from natural language supervision. In *International Conference on Machine Learning*, pages 8748–8763, 2021. 1, 6
- [18] Robin Rombach, Andreas Blattmann, Dominik Lorenz, Patrick Esser, and Björn Ommer. High-resolution image synthesis with latent diffusion models. In *Proceedings of* the IEEE/CVF Conference on Computer Vision and Pattern Recognition, pages 10684–10695, 2022. 6
- [19] Seyedmorteza Sadat, Otmar Hilliges, and Romann M Weber. Eliminating oversaturation and artifacts of high guidance scales in diffusion models. In *International Conference on Learning Representations*, 2024. 1, 4
- [20] Chitwan Saharia, William Chan, Saurabh Saxena, Lala Li, Jay Whang, Emily L Denton, Kamyar Ghasemipour, Raphael Gontijo Lopes, Burcu Karagol Ayan, Tim Salimans, et al. Photorealistic text-to-image diffusion models with deep language understanding. In Advances in Neural Information Processing Systems, pages 36479–36494, 2022. 1
- [21] Jascha Sohl-Dickstein, Eric Weiss, Niru Maheswaranathan, and Surya Ganguli. Deep unsuperviseddeep unsupervised learning using nonequilibrium thermodynamics. In *International Conference on Machine Learning*, pages 2256–2265, 2015. 1, 2
- [22] Jiaming Song, Chenlin Meng, and Stefano Ermon. Denoising diffusion implicit models. In *International Conference on Learning Representations*, 2021. 2, 6, 10
- [23] Yang Song and Stefano Ermon. Generative modeling by estimating gradients of the data distribution. In Advances in Neural Information Processing Systems, 2019. 1, 2
- [24] Yang Song, Jascha Sohl-Dickstein, Diederik P Kingma, Abhishek Kumar, Stefano Ermon, and Ben Poole. Score-based generative modeling through stochastic differential equations. In *International Conference on Learning Representations*, 2021. 1, 2, 3
- [25] Gilbert Strang. Linear Algebra and Its Applications. 2012.
- [26] Wenliang Zhao, Lujia Zhang, Binyan Liu, Ziyu He, Yong Li, Jian Wang, and Jian Bao. Zhao, wenliang and bai, lujia and rao, yongming and zhou, jie and lu, jiwen. In *International Conference on Learning Representations (ICLR)*, 2023. 6

A. Pseudo Code

This section presents the pseudocode for the method. The Algorithm 2 describes the sampling of Full method CFG-EC. The Full method Algorithm 2 presented in the paper is to assign all modified unconditional noise prediction without interpolating with the original unconditional noise prediction output from the existing model.

Algorithm 2 Full CFG-EC

```
1: reverse-time denoising loop
  2: for i = T to 1 do
                extrapolate next-step noises if previous exist
  3.
               if prev_c \neq \emptyset \land \text{prev\_uc} \neq \emptyset then
  4:
                      \begin{array}{l} \operatorname{noise}_{c}^{\operatorname{next}} \leftarrow 2\operatorname{noise}_{c}^{\operatorname{origin}} - \operatorname{prev\_c} \\ \operatorname{noise}_{uc}^{\operatorname{next}} \leftarrow 2\operatorname{noise}_{uc}^{\operatorname{origin}} - \operatorname{prev\_uc} \end{array}
  5:
  6:
                      Initial error vectors
  7:
                      \begin{array}{l} A^{\wedge} \leftarrow \mathrm{noise}_{c}^{\mathrm{origin}} - \mathrm{noise}_{c}^{\mathrm{next}} \\ B^{\wedge} \leftarrow \mathrm{noise}_{uc}^{\mathrm{origin}} - \mathrm{noise}_{uc}^{\mathrm{next}} \end{array}
  8.
  9:
                      Gram-Schmidt to orthogonalize B^{\wedge} to A^{\wedge}
10:
                      B_{\parallel} \leftarrow \operatorname{GramSchmidt}(A^{\wedge}, B^{\wedge})
11:
                      B^{\wedge\prime} \leftarrow B^{\wedge} - B_{\parallel}
12:
                      Modify unconditional noise
13:
                      \operatorname{noise}_{uc}^{\operatorname{mod}} \leftarrow B^{\wedge\prime} + \operatorname{noise}_{uc}^{\operatorname{next}}
14:
                      \text{noise}_{uc} \leftarrow \text{noise}_{uc}^{\text{mod}}
15:
16:
                end if
                CFG mix
17:
                \text{noise\_pred} \leftarrow \text{noise}_{uc} + \omega \cdot \left( \text{noise}_{c}^{\text{origin}} - \text{noise}_{uc} \right)
18:
                \text{prev\_c} \leftarrow \text{noise}_{c}^{\text{origin}}; \text{ prev\_uc} \leftarrow \text{noise}_{uc}^{\text{origin}}
19
20: end for
```

To enable a more accurate estimation of the model's next extrapolation point, we utilize the original unconditional noise prediction as the previous unconditional noise value for the subsequent step.

B. Additional Visual Results

This section presents an extended visual comparison between CFG++ [1] and CFG-EC++. To verify this comparison on high-quality images, we used the latest T2I model, Stable Diffusion XL [16], using the default DDIM sampler [22] with the same seed, prompt and guidance scale ($\omega = 0.6$) 50NFEs.

Looking at Fig. 4, the cactus image (upper left) compared to existing methods, the cactus shows a more realistic representation of the face, a more distinct smile, and the artificial elements on the cheek have been removed. Furthermore, the transparency of the glass and the blood image (upper right) highlight the transparency of the glass, and the blood vessels appear more naturally connected. In the original CFG++ method, soccer matches were

not generated, but our method successfully produced them. Similarly, while the original CFG++ often yielded misaligned mirrors and TV screens, our method achieved proper alignment. As illustrated in the middle-right image, conventional methods (e.g., CFG++) often exhibit artifacts where the firearm's geometry is distorted by features from the subject's clothing, resulting in an unnatural curvature. In contrast, our proposed method generates a more realistic, free from such artifacts. Furthermore, the image in the lower left demonstrates that our approach produces a more realistic scene with enhanced detail in the landscape (e.g., the plains) compared to the baseline. A critical failure mode of the existing method is observable in the lower right image, which incorrectly rendered two tails and three paws on the subject dog. However, our method correctly generates the anatomically accurate count of one tail and two visible paws.

C. Evolution of Denoised Estimates

In this section, we provide a comparison of the progression of denoised estimates generated by CFG-EC and CFG [5]. We employ Stable Diffusion XL (SDXL) with the DDIM sampler using the dynamic method of CFG-EC with 50 NFEs and guidance scale (ω) to 5.0.

In Fig. 5, the top image, corresponding to the prompt "A man gets ready to hit a ball during a baseball game.", demonstrates our method's ability to preserve key objects. While the CFG method fails to retain the baseball bat, our proposed method successfully maintains its presence throughout the sampling process. Similarly, In the middle image, for the prompt "A black piece of luggage with pink writing on it's side." the baseline method fails to apply the "pink writing" attribute, producing an incoherent pink pattern instead of text. Conversely, our method generates distinct pink lettering. Finally, the bottom image, which shows "A black and white picture of a man surfing." reveals a compositional error in the CFG. The CFG method generates an incorrect configuration, with the surfer positioned away from the surfboard. Our method, in contrast, correctly places the surfer on the board, resulting in a more realistic and coherent scene.

Collectively, while the baseline CFG often converges to flawed representations, such as omitting objects, failing to render details, or generating incorrect spatial relationships, our method maintains a more accurate generative trajectory. The corrective mechanism of our approach appears to provide a continuous preventive mechanism that prevents the model from deviating into incorrect states where concepts are improperly merged or details are lost.

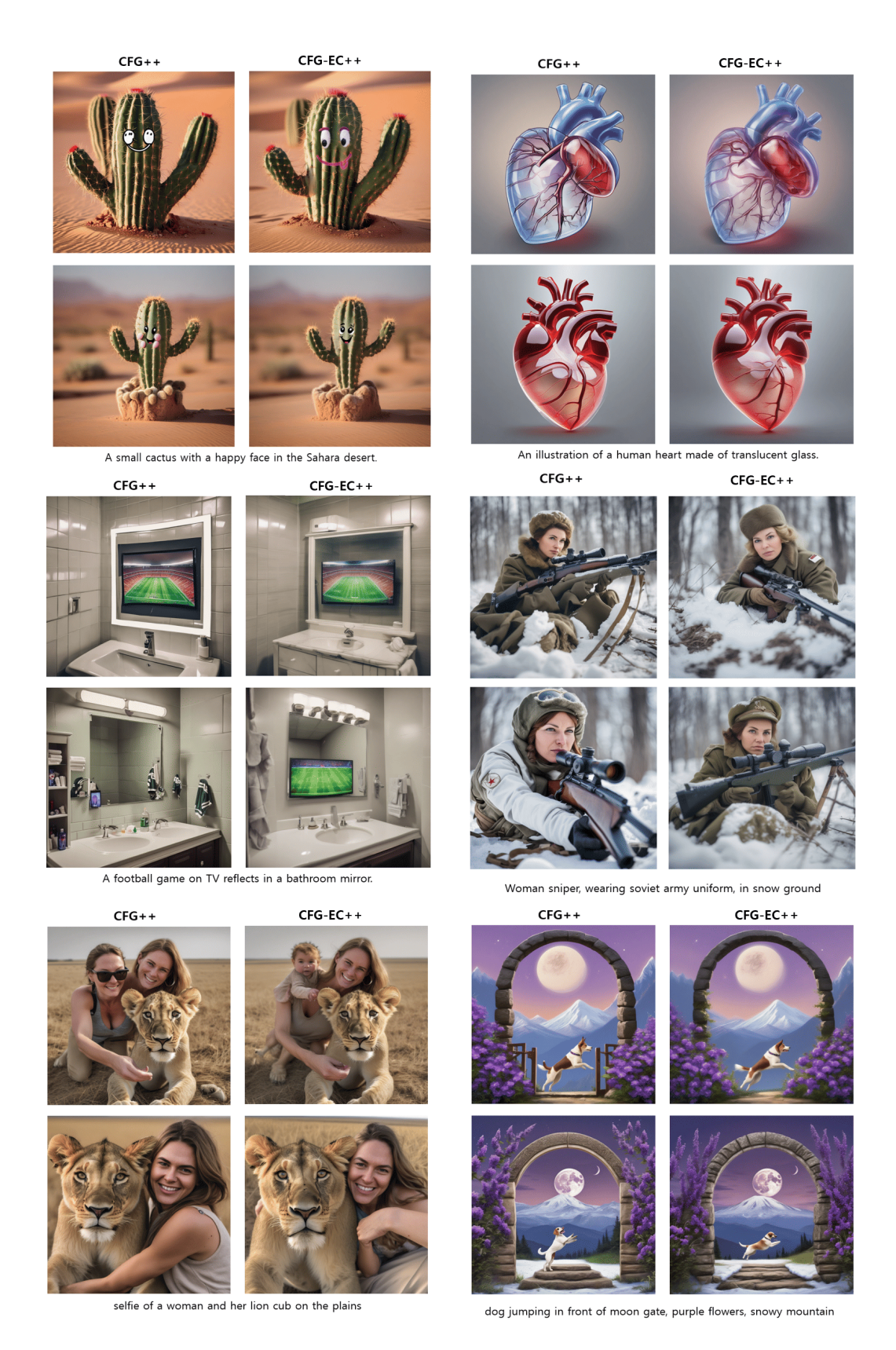


Figure 4. The corresponding SDXL (ω = 0.6) T2I images generated using CFG++ (left) and CFG-EC++ (right) demonstrate improvements. The generated images exhibit fewer artifacts and better prompt alignment.



A man gets ready to hit a ball during a baseball game.



A black piece of luggage with pink writing on it's side.



A black and white picture of a man surfing.

Figure 5. Evolution of denoised estimates generated by SDXL (ω = 5.0). CFG-EC (bottom) shows better adherence to text alignment during the denoising process compared to CFG (top).